aerospace

MDPI

Article

Round-Robin Study for Ice Adhesion Tests

Nadine Rehfeld [1,*], Jean-Denis Brassard [2], Masafumi Yamazaki [3], Hirotaka Sakaue [3], Marcella Balordi [4], Heli Koivuluoto [5], Julio Mora [6], Jianying He [7], Marie-Laure Pervier [8], Ali Dolatabadi [9], Emily Asenath-Smith [10], Mikael Järn [11], Xianghui Hou [12] and Volkmar Stenzel [1]

1 Department Paint Technology, Fraunhofer Institute for Manufacturing Technology and Advanced Materials IFAM, 28359 Bremen, Germany; volkmar.stenzel@ifam.fraunhofer.de
2 Laboratoire International des Matériaux Antigivre/Anti-Icing Materials International Laboratory, Department of Applied Sciences, Université du Québec à Chicoutimi, Saguenay, QC G7H2B1, Canada; jdbrassa@uqac.ca
3 Department of Aerospace and Mechanical Engineering, University of Notre Dame, Notre Dame, IN 46628, USA; myamazak@nd.edu (M.Y.); hsakaue@nd.edu (H.S.)
4 Power Generation Technologies and Materials Department, RSE, Ricerca sul Sistema Energetico, 29122 Piacenza, Italy; marcella.balordi@rse-web.it
5 Materials Science and Environmental Engineering, Faculty of Engineering and Natural Sciences, Tampere University, 33720 Tampere, Finland; heli.koivuluoto@tuni.fi
6 INTA-Instituto Nacional de Técnica Aeroespacial, Área de Materiales Metálicos, Ctra. Ajalvir Km 4, 28850 Madrid, Spain; jmornog@inta.es
7 Department of Structural Engineering, Norwegian University of Science and Technology (NTNU), 7491 Trondheim, Norway; jianying.he@ntnu.no
8 School of Aerospace, Transport and Manufacturing, Centre for Propulsion and Thermal Power Engineering, Cranfield University, Cranfield MK43 0AL, UK; m.pervier@cranfield.ac.uk
9 Department of Mechanical and Industrial Engineering, University of Toronto, Toronto, ON M5S 3G8, Canada; ali.dolatabadi@utoronto.ca
10 US Army Engineer Research & Development Center, Cold Regions Research & Engineering Laboratory, Hanover, NH 03755, USA; emily.asenath-smith@usace.army.mil
11 RISE Research Institutes of Sweden, Department Materials and Surface Design, SE-114 86 Stockholm, Sweden; mikael.jarn@ri.se
12 Faculty of Engineering, University of Nottingham, University Park, Nottingham NG7 2RD, UK; xianghui.hou@outlook.com
* Correspondence: nadine.rehfeld@ifam.fraunhofer.de

Citation: Rehfeld, N.; Brassard, J.-D.; Yamazaki, M.; Sakaue, H.; Balordi, M.; Koivuluoto, H.; Mora, J.; He, J.; Pervier, M.-L.; Dolatabadi, A.; et al. Round-Robin Study for Ice Adhesion Tests. *Aerospace* **2024**, *11*, 106. https://doi.org/10.3390/aerospace11020106

Academic Editor: Ning Zhao

Received: 18 December 2023
Revised: 12 January 2024
Accepted: 14 January 2024
Published: 24 January 2024

Abstract: Ice adhesion tests are widely used to assess the performance of potential icephobic surfaces and coatings. A great variety of test designs have been developed and used over the past decades due to the lack of formal standards for these types of tests. In many cases, the aim of the research was not only to determine ice adhesion values, but also to understand the key surface properties correlated to low ice adhesion surfaces. Data from different measurement techniques had low correspondence between the results: Values varied by orders of magnitude and showed different relative relationships to one another. This study sought to provide a broad comparison of ice adhesion testing approaches by conducting different ice adhesion tests with identical test surfaces. A total of 15 test facilities participated in this round-robin study, and the results of 13 partners are summarized in this paper. For the test series, ice types (impact and static) as well as test parameters were harmonized to minimize the deviations between the test setups. Our findings are presented in this paper, and the ice- and test-specific results are discussed. This study can improve our understanding of test results and support the standardization process for ice adhesion strength measurements.

Keywords: ice adhesion; round-robin; shear test; centrifugal test; Mode I test

1. Introduction

Icephobic surfaces are of great interest for various technical applications, including aviation, energy, and automotive sectors [1–12]. The aim of using such materials is to prevent or delay ice accretions on technical surfaces and/or reduce the adhesion of ice

to the extent that it can be removed easily by external measures (e.g., gravity, vibrations, and heating) without costly energy input. The developers of such icephobic materials are facing a lack of standardized test methods for performance evaluation and technology transition and deployment. Various test methods have been developed over the past decades [13–20], but efforts to compare the test results with each other are limited, resulting in uncertainties of general rules for the identification of icephobic surfaces [21–27]. This study is aimed at the delivery of test data derived from identical coating and tape materials to exclude any uncertainties in the comparability of test surfaces. This includes the selection of robust (mechanical and chemical wise) as well as long-term stable surfaces for the round-robin study.

The use of lab-based tests is generally accompanied by great uncertainty regarding the significance of test results in terms of their final technical application. Some researchers have suggested different values for low ice adhesion coatings, including Hejazi et al. (2013), who suggested a threshold of 100 kPa [28], and Dou et al. (2014), who suggested a value of $\tau_{ice} \leq 27$ kPa for ice detachment by a strong breeze [29]. The data contrast with the test data summarized by Work and Lian (2018), with averaged values for aluminum (a non-icephobic material) ranging from 27 to 122 kPa for centrifuge tests [22]. Other researchers have introduced the so-called adhesion reduction factor (ARF) by dividing the adhesion strength of a predefined benchmark material by that of the test surface [13]. This accounts for the nonuniform stress distributions during ice adhesion tests and allows for comparison against a state-of-the-art material. In this case, the data quality of the benchmark material needs to be at a certain level (standard deviations preferably below 10%) to avoid any misinterpretations. Nonetheless, it is uncertain whether it will be possible to define general values that are valid for all types of ice adhesion tests and ice adhesion thresholds in the future. This is not only due to the different test designs but also because of the variable and complex (de-)icing scenarios of the target applications. However, this study aims to deliver ice adhesion strength data for defined surfaces, allowing the comparison of test designs and the development of steps to lead future research topics.

The different types of ice adhesion measurements vary in fundamental principles regarding how the ice is formed and removed. Additionally, variances in temperature and test duration result in further deviations in ice adhesion values [30]. Conducting different ice adhesion measurements under harmonized test conditions and on identical test surfaces will allow the comparison of these results and improve the understanding of differences in test designs. Table 1 summarizes the contributors in this paper.

Table 1. List of contributors to the ice adhesion round-robin tests.

Institution	Used Abbreviation	Country	Ice Type	Test Type
Power Generation Technologies and Materials Department	RSE	Italy	Static	Shear: pull
Instituto Nacional de Técnica Aeroespacial	INTA	Spain	Static	Shear: pull
RISE Research Institutes of Sweden	RISE	Sweden	Static	Shear: pull
Norwegian University of Science and Technology	NTNU	Norway	Static	Shear: push
University of Notre Dame	ND	USA	Static	Shear: push
Cold Regions Research & Engineering Laboratory	CRREL	USA	Static	Shear push and tensile peel
Université du Québec à Chicoutimi	AMIL	Canada	Static + impact	Centrifuge
Fraunhofer IFAM	IFAM	Germany	Static + impact	Centrifuge
University of Nottingham	NU	UK	Static	Centrifuge
Tampere University	TAU	Finland	Impact	Centrifuge
Partner-A	P-A	---	Impact	Centrifuge
Concordia University	ConU	Canada	Impact	Mode I
Cranfield University	CU	UK	Impact	Mode I

This paper summarizes the results of ice adhesion measurements in the various test facilities on identical test surfaces. The test surfaces were proven to possess appropriate stability over the period of testing in a parallel study [31]. The results are grouped with

regard to the test types and ice types, compared to each other, and the observed similarities and differences are discussed.

2. Materials and Methods

Neither standard test methods nor general parameter sets were available for the ice adhesion tests. To conduct round-robin tests, basic test types were identified, and test parameter sets were defined to achieve maximum comparability of the test results. The test surfaces and pretreatment procedures (handling and cleaning) were identical in order to exclude any further deviations from the test types.

2.1. Test Sample Preparation

The sizes and geometries of the test samples differed due to the various test designs in this round-robin test. Prior to coating application, all test samples were sanded (3M 320-grit sandpaper) and cleaned with isopropanol. The preparation of the samples for this round-robin test was performed in a single process with identical material batches to avoid deviations due to changes in material composition, handling, or environmental conditions. We used four different test surfaces that represented a general range of wettability and roughness and that were proven to be robust in a previous study [31]. The chemical (for cleaning purposes) and mechanical (for repeated icing/de-icing cycles) stability assured a high comparability of the test surfaces for the different test facilities.

For the coating type "Primer", an epoxy primer (Aerodur 37045 Barrier Primer White with Hardener S66/22R; Akzo Nobel, Sassenheim, The Netherlands) was used in a mixing ratio of 2:1 by volume. Material preparation and application were carried out according to supplier specifications using a spray gun (SATA Jet 90 with Ø 1.3 mm, pressure of 1.6 bar, and distance of 40 cm) under standard conditions (temperature of 21 °C and relative humidity of 40%). After the coating application, samples were stored at room temperature in a clean environment for 12 h prior to thermal curing at 60 °C for 60 min. The resulting dry film thickness of the primer was 40 ± 10 µm (according to DIN EN ISO 2808:2019 with byko-test 8500 P Fe/NFe, Byk Gardner, Geretsried, Germany) [32]. Figure 1 shows the test samples after primer application.

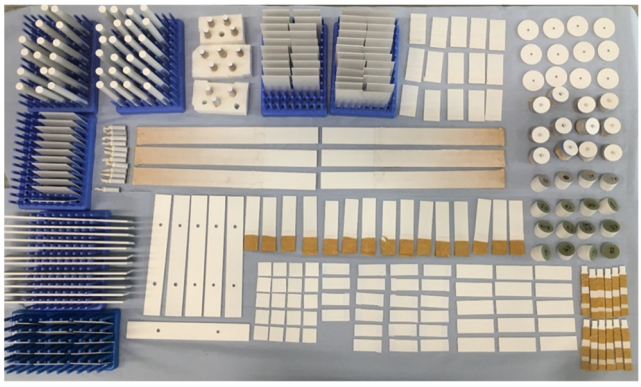

Figure 1. Test samples for the round-robin study after primer application.

The coating type "Standox" is a clear coat that is used for repairs in the automotive industry. It was applied on top of the primer coating (described above) to ensure good adhesion properties. Standocryl VOC-Premium Clear K9540 with Hardener VOC 10–20 was purchased (Standox GmbH, Wuppertal, Germany), and material preparation was carried out according to supplier specifications in a mixing ratio of 3:1 (by volume). Application and curing parameters were identical to those of the primer coating. The same application method was used for the coating type "PUR C25", which is a noncommercial 2-component formulation based on silanized polyisocyanate-curing acrylic resin as described in [33]. The total film thickness (incl. primer) for the samples Standox and PUR C25 was 70 ± 15 µm [32].

The last material in this study was "PTFE Tape" (extruded polytetrafluoroethylene PTFE film tape 5490; 3M Deutschland GmbH, Neuss, Germany) which was applied on primed test samples according to supplier specifications. The film thickness of the tape was 90 µm.

Samples for 15 partners were prepared as described and delivered by Fraunhofer IFAM. Additionally, CRREL prepared test samples as follows: The materials of interest (Primer, Standox, PTFE tape) were applied to aluminum substrates for testing. Before the coating application, all aluminum substrates were polished with lapping films through p4000-grit papers, resulting in an average roughness of approximately 0.362 µm, measured using a non-contact optical profilometer (Model ST400, Nanovea, Irvine, CA, USA) equipped with a confocal chromic sensor (ISO 25178). Following the polishing process, the substrates were rinsed with high-purity water, dried with ethanol, and stored in airtight bags until used for coating or testing. At the time of use, substrates were removed from the sealed bags, soaked in sulfuric acid (pH 1.5) for 5 min, rinsed with high-purity water, and then dried by wiping with acetone or isopropanol. The substrates were then tested for ice adhesion or had coatings applied within 30 min to limit the formation of aluminum oxide on the surfaces. All coatings were applied and cured according to manufacturer specifications.

2.2. Surface Characterizations

For the assessments of the ice adhesion, we selected 4 different materials that represented a reasonable range of wettability and roughness properties and that were proven to be robust in repeated tests, as reported in [31]. Surface characterization was conducted prior to the shipment of the test samples to the partners for ice adhesion measurements. Wettability tests were performed with the Drop Shape Analyzer DSA 100S (Krüss GmbH, Hamburg, Germany), according to relevant specifications (DIN EN ISO 19403-2) [34]. Surface free energy (SFE) was determined by measuring the dynamic contact angle of 3 liquids—water, diiodomethane, and ethylene glycol (droplet application of 0.2 µL/s and a total volume of 6.0 µL)—and calculated according to the method of Owens, Wendt, Rabel, and Kaelble (OWRK). The water contact angle (WCA) was extracted from this measurement. The water sliding angle (WSA) was determined with a water droplet volume of 20 µL and a tilting speed of 60°/min. The sliding angle was defined as the angle at which the advancing and receding angles of the water droplet moved at least 1 mm from the starting point [35]. Contact angle hysteresis (CAH) was determined at this sliding angle or at the maximum tilting angle of 90° (in the case where the water droplet did not run off) by calculating the difference between advancing and receding angles. The tilting method was chosen because it delivers consistent results. Roughness data R_a (arithmetic average value of the roughness profile) and R_z (maximum height of the profile) were determined using a Perthometer M2 (Mahr GmbH, Göttingen, Germany). Surface parameters are expressed in Table 2 as the means of 6 measurements from 3 test samples. Additional random samples for each participating partner were controlled against these data to demonstrate the comparability of delivered test samples of this series.

Table 2. Surface properties of the 4 selected materials (IFAM preparations).

	Primer	**Standox**	**PUR C25**	**PTFE Tape**
SFE (mN/m)	38.5 (±0.3)	36.0 (±1.0)	18.0 (±0.8)	15.1 (±0.4)
WCA (°)	83 (±1)	86 (±1)	100 (±1)	110 (±2)
WSA (°)	>90	67 (±4.7)	41 (±2.8)	29 (±3.4)
CAH (°)	40 (±2.3)	36 (±3.1)	26 (±1.8)	22 (±2.1)
R_a (µm)	1.5 (±0.07)	0.07 (±0.007)	0.05 (±0.010)	0.11 (±0.015)
R_z (µm)	8.3 (±0.26)	0.38 (±0.035)	0.29 (±0.038)	0.68 (±0.088)
Description:	Hydrophilic roughness: high	Hydrophilic roughness: low	Hydrophobic roughness: low	Hydrophobic roughness: moderate

At CRREL, wettability experiments were performed with a Model 590 contact angle goniometer (Ramé-Hart, Succasunna, NJ, USA) with an automated liquid dispensing system, tilting base, and camera using the Dropimage Advanced software package. Six measurements were performed for each material surface. For sliding (WSA) and static (WCA) contact angle measurements, 20 µL of MilliQ® was dispensed onto the material surface. Static angle measurements were determined from the initial contact angle measurement prior to tilting at t0. Tilting of the base for WSA measurements was performed at 60° per min (1° per second) with automated measurements performed every 0.5 s. The sliding angle was determined at the point when the leading edge of the drop slid out of the camera's frame (approximately 1 mm of movement from the initial position), and the volumetric measurement for the drop determined using the Dropimage Advanced software fell below 20 µL. Contact angle hysteresis was calculated using the trailing and leading contact angle from 1 measurement prior to the drop moving out of the frame and volumetric measurement reduction.

Roughness was determined by obtaining 1 × 1 mm scans using the optical profilometer (described above) in a 5 µm step size in both x and y directions. The scanned surfaces were analyzed using MountainsMap 7.4. The surface form was removed using a 2nd-order polynomial fit. Using the removed surface form, 6 horizontal profile lines (in the direction of scanning) were extracted at equidistant lengths. Roughness and waviness from the extracted profile were separated using a Gaussian filter with a cut-off of 250 µm, and R_a and R_z values were reported. Results are summarized in Table 3.

Table 3. Surface properties of the 3 selected materials (CRREL preparations).

	Primer	**Standox**	**PTFE Tape**
WCA (°)	87 (±4.7)	88 (±4.1)	95 (±1.5)
WSA (°)	88 (±4.6)	57 (±7.5)	35 (±2.5)
CAH (°)	30 (±16.0)	35 (±5.4)	20 (±1.9)
R_a (µm)	0.49 (±0.02)	0.67 (±0.21)	0.09 (±<0.01)
R_z (µm)	2.36 (±0.07)	6.92 (±1.38)	0.53 (±0.03)
Comparison with IFAM preparation:	Wettability: comparable, roughness: lower	Wettability: comparable, roughness: higher	Wettability: lower, roughness: comparable

Results for test surfaces, prepared by IFAM, indicate surface free energies (SFE) from 15.1 mN/m to 38.5 mN/m (Table 2). Water contact angles (WCA) were determined from 83° to 110°. This property range was expected to be sufficient for the round-robin study. A further increase in wettability (higher SFE and lower WCA) bears the risk of cohesive ice failure instead of quantifiable ice adhesion results. For surfaces with lower wettability (lower SFE and higher WCA, including superhydrophobic surfaces), no materials were identified that fulfilled the requirements for this round-robin study in terms of robustness and long-term stability.

The comparison of the resulting surface properties from CRREL and IFAM preparations showed significant deviations in roughness for the Primer and Standox coating materials. This may be caused by differences in the used substrates, material batches, and application techniques. For the CRREL preparation, the Primer surface showed a significantly lower roughness, but the Standox material showed an increased roughness. For the PTFE tape, the roughness data are in a comparable range, indicating no effects based on the different roughness measurement techniques but showed differences between the coating types for CRREL and IFAM preparations. The trends for contact angle measurements fit well despite the different methods. The only significant difference was observed for the WCA of PTFE tape (CRREL 95° and IFAM 110°), which may be the result of static and dynamic contact angle measurements using different volumes and fitting methods. These findings will be considered during the result assessments for the ice adhesion data and emphasize the need to prepare test samples for comparison tests in a single facility.

2.3. Ice Adhesion Test Methods

The test methods in this study cover a wide range of designs and are grouped into direct mechanical tests (push or pull), centrifuge tests, and mode I tests, as described below.

2.3.1. Direct Mechanical Tests (RSE, INTA, NTNU, RISE, ND, and CRREL)

The described tests used static ice for the assessment of ice adhesion; graphical schemes and images are summarized in Table 4.

Table 4. List of direct ice adhesion test methods used by the round-robin contributors.

RSE pull test device	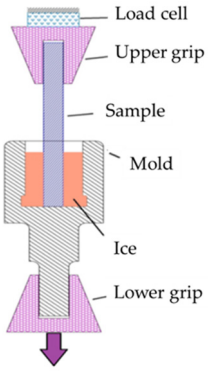	
INTA double-lap shear test	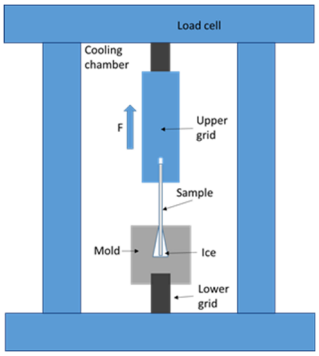	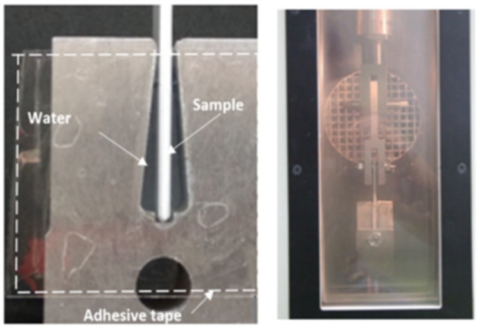
RISE modified slip/peel method	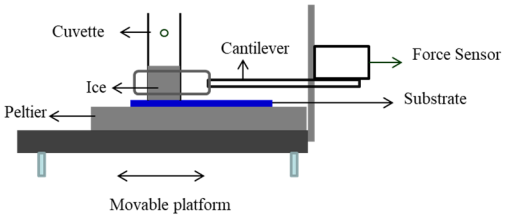	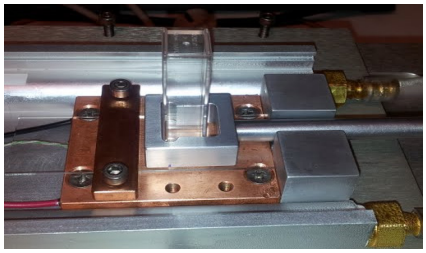

Table 4. *Cont.*

NTNU vertical shear test	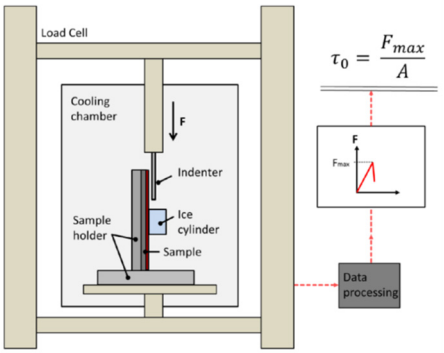	
Notre Dame (ND) push test device	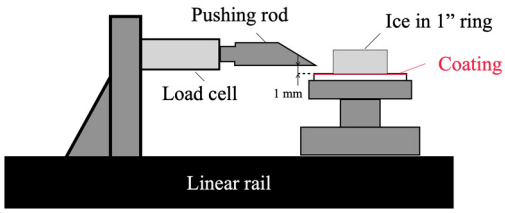	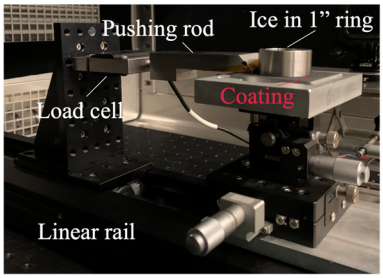
CRREL ice adhesion peel test–shear test method	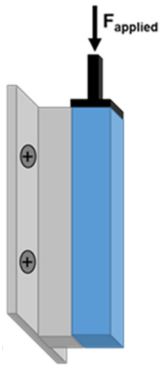	
CRREL ice adhesion peel test–tensile test method	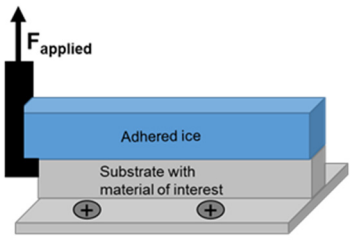	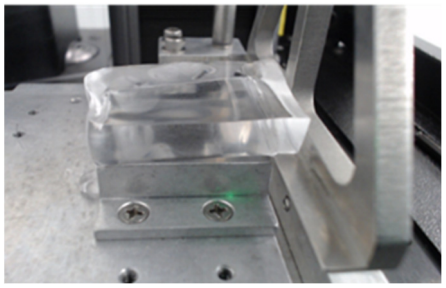

RSE conducted direct mechanical tests by using a homemade apparatus for shear test in pull mode equipped with an electromechanical testing system, INSTRON 4507 [36]. The specimens with a cylindrical shape were frozen in an aluminum alloy mold at −19 °C overnight, and then the mold was fixed into the machine and the sample was extracted

from the ice at a speed of 0.3 mm/s. The force F needed to pull the sample off the mold was recorded.

INTA's double-lap shear (pull) method is a modification of a test described by Ferrick et al. (2006) [37] in which optimizations have been adapted: The dented edges of the mold were replaced by wedge-shaped molds, which helped to decrease the cohesive ice fracture tests that were probably caused by the stress generated by the upward-slanting roughness elements. Regarding the method, the ice was prepared in-mold using adhesive tape to retain the deionized water and the coupon; the ice was frozen at −8 °C overnight inside an ultra-low temperature freezer (Arctiko ULTF series). One hour before the test, the adhesive tape was removed, and any remaining ice accreted over the sample edges was carefully but quickly removed using a blade. The molds were placed in the freezer again for 1 additional hour. The test blocks prepared using this method were then fixed to an Instrom 5882 Universal Machine and placed inside a climate chamber (refrigerated with liquid nitrogen). The samples were left for 5 additional minutes before beginning the test in order to stabilize the temperature. The displacement speed was set to 0.3 mm/s, and the test was initialized until the samples were completely out of the mold. The F_{max} value of the loading curve was used to calculate the ice adhesion strength.

At RISE, an ice shear test (pull mode) was performed by using a plastic cuvette attached to the surface with an inverted lab jack and filled with 1 mL of ultraclean water (Milli-Q, Type 1) through a hole in the cuvette [38]. The assembly was then placed in a freezer (−8 °C) for 180 min. The ice adhesion strength was measured with a modified slip/peel tester (IMASS SP-2000) equipped with a force sensor and a Peltier cooling plate. The equipment was kept in a climate room at 23 °C and 50% RH. Immediately prior to the measurement, the sample was transferred from the freezer to the Peltier plate, which was maintained at −8 °C.

NTNU measured ice adhesion strength by vertical shear test rig (push mode) using an Instron 5944 Universal Machine equipped with a home-built cooling chamber and testing system. A polypropylene tube mold with a 1 mm-thick wall and a 28 mm inner diameter was placed onto the coatings acting as an ice mold; then, the pressure of a 200 g metal cylinder was applied to prevent water leakage. Subsequently, 5 mL of deionized water was syringed into the mold, and the mold was transferred into a freezer at −8 °C for 180 min to ensure complete freezing. Before the test, the samples were transferred from the freezer to the cooling chamber and stabilized at −8 °C for 30 min. During ice adhesion tests, a force probe with a 5 mm diameter propelled the tube-encased ice columns at a velocity of 0.3 mm s^{-1}, and the probe was located close (less than 1 mm) to the tested coating surface to minimize the torque on the ice cylinder. The loading curve was recorded, and the peak value of the shear force (F_{max}) was used for the calculation of the ice adhesion strength.

ND employed a horizontal push-type device to measure the ice adhesion. On the test sample plate, the ice was created inside an aluminum ring with a 1 inch inner diameter. The ring with the ice was then pushed horizontally using a rod that was attached to the load cell. The output voltage reading of the load cell was converted into the force to determine the ice adhesion. During the measurement, the ambient temperature was kept at −8 °C, and the pushing speed was controlled at 0.3 mm/s.

For ice adhesion tests conducted by CRREL, freshwater columnar ice was grown on the substrates [39]. This method did not use molds to facilitate surface freezing, but used a growth from the melt procedure instead. Ice growth was conducted at −8 °C. Under these conditions, approximately 1.5 h was required to grow the 1 cm-thick laminate of ice on the material surfaces. The ice adhesion peel test (IAPT) developed at CRREL [40] was carried out in tensile or shear delamination modes. In the tensile mode, the ice is lifted away from the substrate; in the shear mode, the ice is pushed off the substrate along its surface. The testing geometry was fitted inside a universal load frame with machined baseplates and custom load heads. Load and displacement were recorded as a function of time during the test.

For the calculation of the ice adhesion strength (τ_0), the following equation was used by all contributors,

$$\tau_0 = \frac{F_{max}}{A}, \quad (1)$$

where F_{max} is the maximum force and A is the contact area at the ice substrate interface. Quantitative results indicate that the ice was delaminated by purely adhesive mechanisms with no residual ice remaining on the material surfaces after testing. The ice laminate was removed as a single piece without cohesive failure. A summary of methods for ice adhesion measurements using direct mechanical tests is provided in Table 4.

2.3.2. Centrifuge Tests (AMIL, IFAM, NU, TAU, and P-A)

The contributors AMIL, IFAM, and NU conducted centrifuge tests using static ice. Additionally, AMIL, IFAM, TAU, and P-A used impact ice, accreted in ice wind tunnels, for the assessments. Generally, the centrifuge test used centripetal forces to apply shear stress to the ice and remove it from the test surface. Separation is detected when the ice hits the centrifuge wall and is correlated to the rotational speed of the centrifuge rotor. This speed (angular velocity ω in rad/s) was used to calculate the shear strength of ice to the substrate according to the following equation,

$$\tau = \frac{F}{A} = \frac{m_{ice}\,\omega^2\,r}{A}, \quad (2)$$

where m_{ice} is the mass of ice (kg), r is the radius of the rotating beam at the mid-length ice position (m), and A is the surface area of the adherent interface (m^2) [13]. The calculated values express the adhesive strength of the ice. This method is specified in ISO/TS 19392-6:2023 [41].

AMIL conducted centrifuge tests with static and impact ice. The tests were performed using 32 mm-wide × 6.4 mm-thick aluminum 6061-T6 flat bars cut to a 340 mm length; the surface materials for this round-robin study were tested in a cold chamber, a closed-loop icing wind tunnel, and a centrifuge to conduct the tests under controlled environmental conditions. Figure 2 summarizes the test equipment used at AMIL [19].

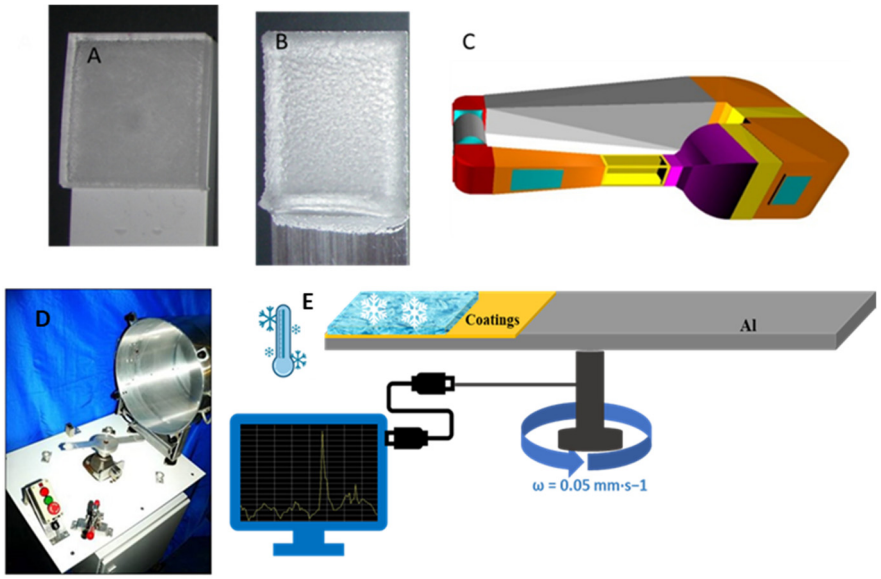

Figure 2. General view of the test equipment at AMIL. (**A**,**B**) are static and impact ice substrates, respectively. (**C**) shows a general view of the AMIL closed-loop ice wind tunnel. (**D**) shows a general view of the CAT vat. (**E**) shows the view inside the centrifuge.

IFAM conducted centrifuge tests with static and impact ice. Test samples (EN AW 5083, dimensions of 220 mm × 30 mm × 4 mm) with the surface materials of this round-robin

study were tested in an ice lab that includes a closed-loop ice wind tunnel and a centrifuge to conduct the tests under controlled environmental conditions. Figure 3 summarizes the test equipment used at IFAM.

(**a**) (**b**) (c)

Figure 3. View inside the Fraunhofer IFAM ice lab with closed-loop ice wind tunnel. (**a**) Test sample preparation for ice accretion using a silicone mold (static ice, (**b**) **left**) or a specimen holder for ice wind tunnel insertion (impact ice, (**b**) **right**). (**c**) View inside the centrifuge with test sample with ice formation (**upper**) and test sample after fixation (**lower**).

NU measured the ice adhesion strength using the centrifugal method with static ice. The coated specimens possessed dimensions of 50 mm × 20 mm × 1 mm, and the test was conducted in an environmental chamber (ALPHA 1550-40H) with controlled temperature (e.g., −8 °C). Glaze ice was formed on the coating surface with a silicone mold. The mold was kept on top of the ice block during the test, and its weight was also counted for the calculation. Figure 4 illustrates the schematic diagram of the formation of the glaze ice and the testing configuration at NU.

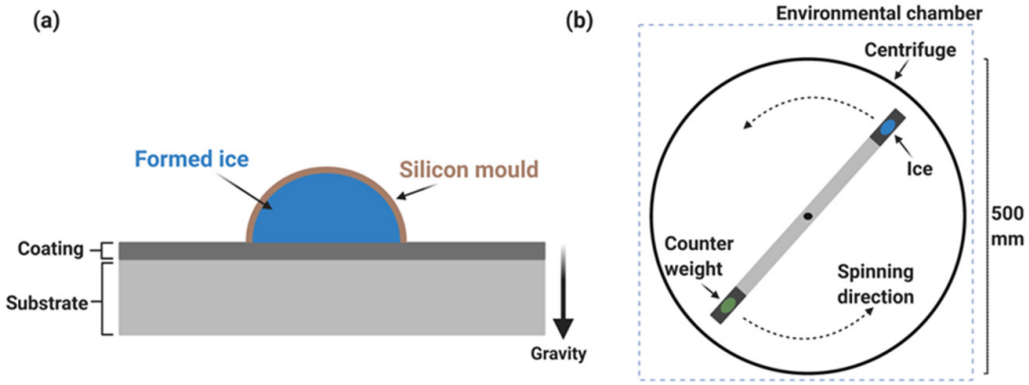

Figure 4. (**a**) Glaze ice formation on a sample surface and (**b**) the testing configuration using the centrifuge method at NU (adapted from [42]).

Ice accretion and centrifugal ice adhesion tests (CATs) were performed at the Ice Laboratory at TAU. Ice was accreted with an icing wind tunnel (IWiT) which is located in a climate-controlled cold room. Figure 5 shows icing test facilities, and more information can be found in [43]. Ice was accreted on flat samples in an area of 30 mm × 30 mm. Typically, in TAU's icing tests, a wind speed of 25 m/s, a temperature of −10 °C in the IWiT, and an acceleration speed of 300 rpm/s were used in the CATs. Similar to previous studies, mixed glaze-type ice was used [44], but in this present study, the parameters in the iWiT were selected as wind speed of 15 m/s and temperature of −8 °C. In the CATs, 200 rpm/s was used as an acceleration speed for the test samples.

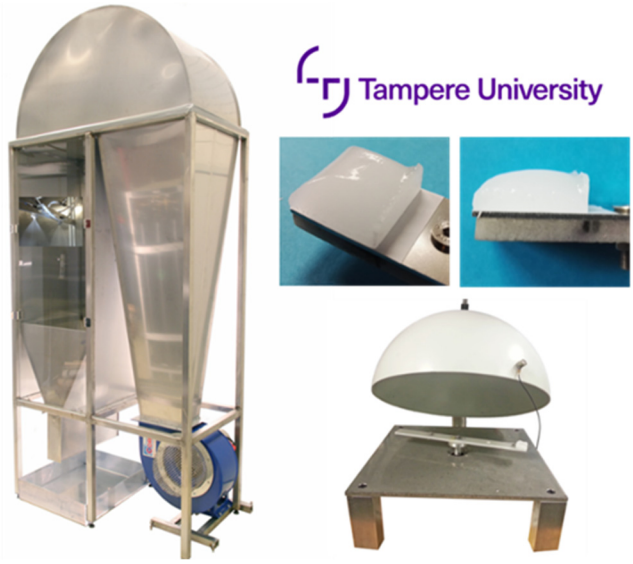

Figure 5. Icing wind tunnel (IWiT), centrifugal ice adhesion tester (CAT), and examples of mixed glaze ice accreted on test samples at Tampere University (TAU), Finland.

2.3.3. Mode I Tests (CU, ConU)

Mode I tests were conducted by 2 participants, Cranfield University (CU), UK, and Concordia University (ConU), Canada, in their respective icing wind tunnels [45,46] using impact ice. Both test devices are similar in principle and were adapted from the Andrews and Lockington blister test [47,48]. The device used in this test consisted of a hollow cylinder of 30 mm (CU) or 40 mm (ConU) in diameter with an inner hole of 4 mm in diameter. In the CU device, the cylinder was made of aluminum 2024-T3 with a front face coated with the material under investigation. Alternatively, in the ConU setup, the cylinder was used as a sample holder where the coated substrates could be secured on the surface using a cap, as shown in Figure 6c.

The inner hole of the cylinder was covered by a thin PTFE disc of 6 mm in diameter and 50 µm in thickness (CU) or a thin rubber elastomer flushed to the surface of the substrate (ConU) prior to testing. This acted as a defect to initiate a crack at the ice/substrate interface as well as to cover the hole to avoid unwanted ice accretion (Figure 6b).

The devices were positioned in the test section of the icing wind tunnel at CU and ConU such that the coated surfaces were perpendicular to the airflow (Figure 6a,d). Ice was accreted on the front surface, and when a sufficient thickness was obtained to ensure plain stress condition, gas was allowed through the hole with gradually increasing pressure until ice detached from the substrate. The thickness of ice prior to removal was 15–20 mm for both CU and ConU. The spray was left on during the entire mechanical test. The type of fracture (adhesive, cohesive, or mixed) as well as the critical pressure needed to remove the ice were monitored and used to calculate the fracture energy and the tensile strength of the ice. Separation was detected when there was a drop in the pressure rise of the applied force.

The fracture energy (FE) required to open the crack can be calculated from the critical pressure P_c, the thickness of ice, and the size of the flaw [48,49]. The fracture toughness and the tensile strength can be obtained from the fracture energy using the average grain size as a typical defect size (Equation (3)),

$$\sigma_T = \sqrt{\frac{FE \times E_i}{(1-\nu_i)^2}} \times \frac{1}{\sqrt{\pi \times a_g}}, \quad (3)$$

where E_i and ν_i are the Young's modulus and the Poisson ratio of ice, respectively, and a_g is the average grain size of the ice [48].

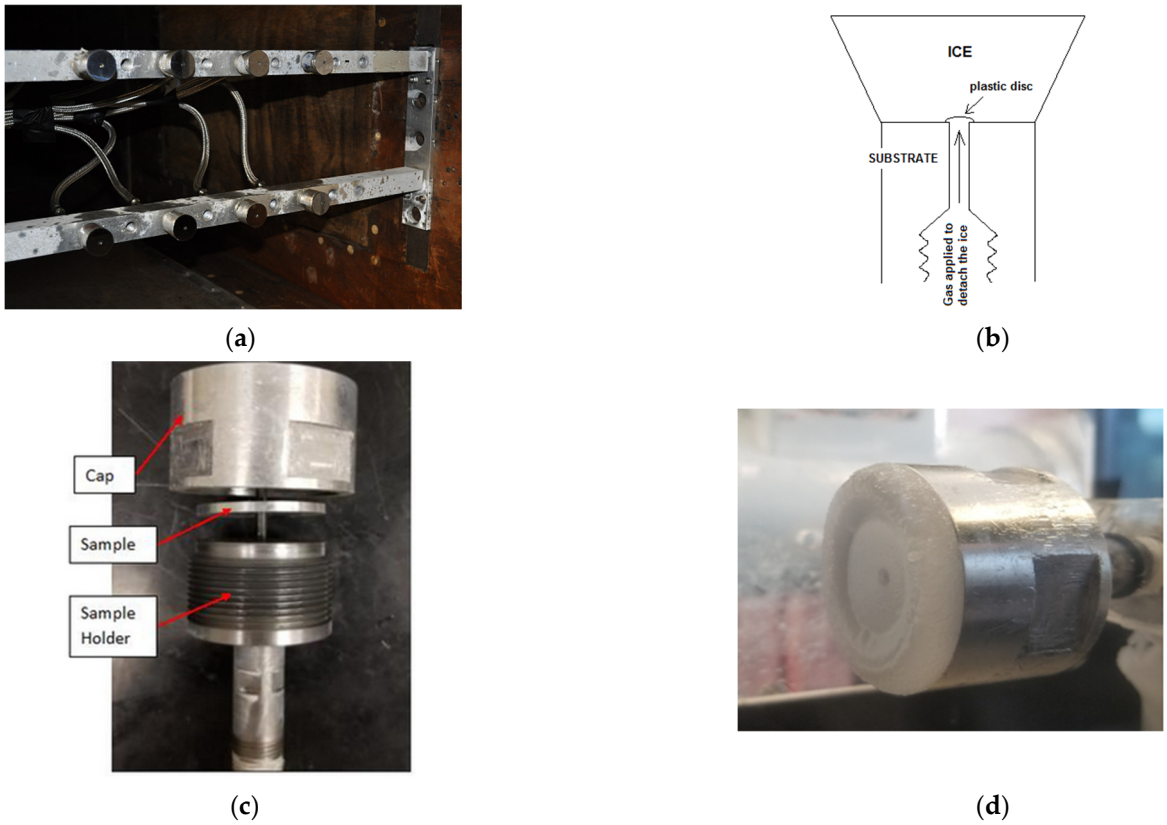

Figure 6. Mode I test rig installed in Cranfield icing wind tunnel (**a**), schematic drawing of the device used by CU (**b**), Mode I sample holder used by ConU (**c**), and ice accretion process on the substrate (**d**).

2.4. Test Parameter Definition

For ice adhesion measurements, test conditions and resulting ice types are of high relevance for data interpretation. In this study, ice formation types were divided into "static ice" and "impact ice". Static ice refers to ice that is formed from liquid water, poured in a mold or alike, and allowed to freeze directly onto the test surface. Impact ice refers to ice accretions, formed in an ice wind tunnel with impacting water droplets onto the test surfaces, leading to the formation of an ice layer for subsequent ice adhesion testing. Icing conditions as well as parameters for the ice removal during the tests were discussed between the partners and coordinated to obtain the greatest conformity possible.

Regardless of the method used, all test surfaces were cleaned prior to testing by using isopropanol and soft tissue. This was defined in a pre-phase of the round-robin study along with further basic parameters: The temperature for all tests was set to −8 °C, and deionized water was used unless otherwise stated in Tables 5 and 6. This harmonization was conducted to improve the comparability of test results.

Table 5. Summary of test parameters for tests using static ice.

	Test Facility	Test Name	Sample Geometry	Iced Area [cm^2]	Freezing from...	Ice Characterization	Temp. [°C]	Icing Time [min]	De-Ionized Water	Handling of Iced Samples	Conditioning Time after Sample Handling: X min	Test Temp. [°C]	Test Specific Information
PULL	RSE	shear: pull	cylindrical	17.02	Aluminum molds	clear ice: mass 50 g	−8	overnight	✓	Y	5	−8	Ice formation −19 °C; displacement speed: 0.3 mm/s
	INTA	Double lap shear	flat	17.5	bulk water, sealed mold sides	clear ice, mass 3.5 g		overnight	✓	Y	5		displacement speed: 0.3 mm/s
	RISE	shear: pull	flat	1	bulk waterplastic cuvette	clear ice mass: 0.9 g/sample		180	✓	Y	2–5		displacement speed: 0.3 mm/s
PUSH	NTNU	ice shear test	flat	6.15	bulk water, poly-propylene molds sealed by silicone	clear ice	−8	120	✓	Y	5	−8	displacement speed: 0.3 mm/s
	ND	shear: push	flat	5.07	water in steel ring (Ø 1 inch)	clear ice		180	✓ (distilled)	Y	5		displacement speed: 0.3 mm/s
	CRREL	peel test (shear)	flat	12	Mold free crystallization from the melt	clear ice, columnar		90	✓	N	5		displacement speed: 0.01 mm/s
TENSION	CRREL	peel test (tension)	flat	12	Mold free crystallization from the melt	clear ice, columnar	−8	90	✓	N	5	−8	displacement speed: 0.01 mm/s
CENTRIFUGE	AMIL	centrifuge	flat	11.2	bulk water silicone moulds	clear ice, about 7 g	−8	35	✓	Y	20	−8	Radius 17 cm; acceleration 300 rpm/s
	IFAM	centrifuge	flat	9	bulk water silicone moulds	clear ice, mass 3 g		90	✓	Y	15		Radius 11 cm; accelaration 200 rpm/s
	NU	centrifuge	flat	1.38	bulk water silicone moulds	glaze ice, mass 1.31 g		180	✓	Y	5		Radius 16.75 cm; acceleration 30 rpm/s

Table 6. Summary of test parameters for tests using impact ice.

	Test Facility	Test Name	Sample Geometry	Iced Area [cm^2]	Freezing from…	Ice Characterization	Temp. [°C]	Velocity [m/s]	LWC [g/m^3]	MVD [μm]	De-Ionized Water	Handling of Iced Samples	Conditioning Time after Sample Handling: X min	Test Temp. [°C]	Test Specific Information
CENTRIFUGE	AMIL	centrifuge	flat	11.2	supercooled droplets	8 mm (±2 mm) thick	−8	15	0.8	27	✓	Y	10	−8	Radius 17 cm; acceleration 300 rpm/s
	TAU	centrifuge	flat	9	supercooled droplets	~9.5 mm thick; ice mass~8 g		15	0.8	20	✓	Y	17 h		Radius 17 cm; acceleration 200 rpm/s
	IFAM	centrifuge	flat	9	supercooled dorplets	~4 mm thick; ice mass~3 g		40	1.3	20	✓	Y	15		Radius 11 cm; acceleration 200 rpm/s
	P-A	centrifuge	not specified	10	supercooled droplets	ice mass 9–10 g		40	0.5	20	✓ (distilled)	N	not specified		Radius 18.5 cm, acceleration 150 m/s
MODE I	ConU	Mode I	cylinder end	12.6	ice wind tunnel	10 mm thick	−8	40	0.5	20	✓	N	"spray on" during testing	−8	pressure rise 10 bar/s
	CU	Mode I	cylinder end	7.07		15 mm thick		40	0.5	20	✓	N			

3. Results

The results of this study are presented in subsections, following the structure of the previous Section 2.3. The results section includes graphs with means and standard deviations for each test method and the tested materials. Raw data are included in the Appendix A.

3.1. Direct Mechanical Tests Using Static Ice (RSE, INTA, NTNU, RISE, ND, and CRREL)

For the mechanical ice adhesion tests, seven methods were used by six different laboratories. Figure 7 summarizes the results by indicating mean and standard deviations of the measurement data, based on the raw data, included in Appendix A—Table A1.

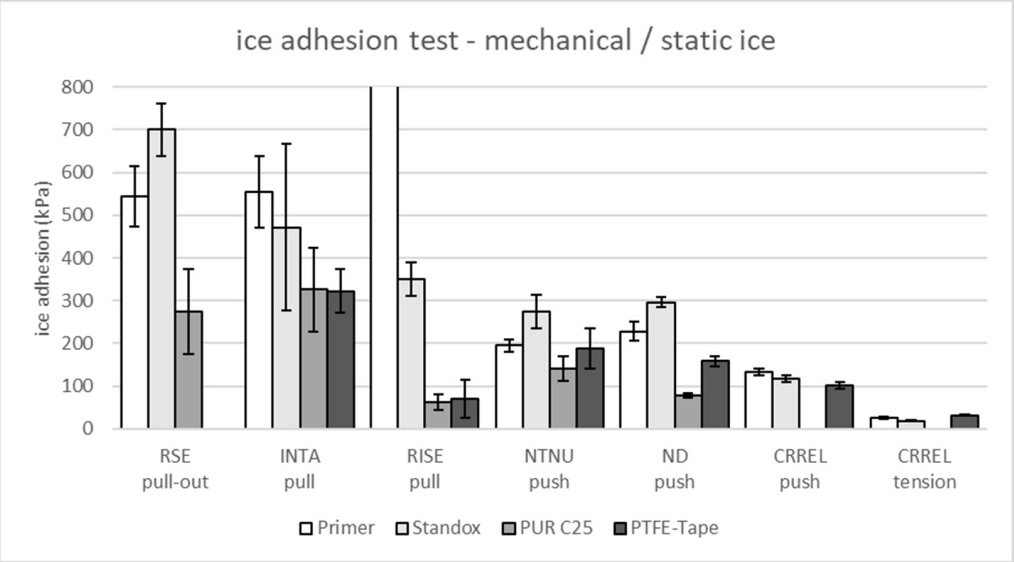

Figure 7. Results for mechanical ice adhesion tests using static ice. Bar exceeding the ice adhesion axis refers to the qualitative result: high ice adhesion strength, resulting in cohesive ice failure.

The results for mechanical ice adhesion tests show the highest data range for the Primer and Standox coating materials: from cohesive failure (RISE) to 26 kPa (CRREL, tension) and from 700 kPa (RSE) to 19 kPa (CRREL, tension) for the Primer and Standox materials, respectively. These coating materials were expected to have no low ice adhesion properties, resulting in higher ice adhesion strengths compared to the PUR C25 and PTFE tape materials. This is shown by the pull- and push-based shear tests in this study. The standard deviations were comparably high for the INTA results. The result discrimination was less distinct for the NTNU results. However, all test results derived from the materials prepared and delivered by Fraunhofer IFAM confirmed the basic expectations in the ice adhesion ranking.

For CRREL, it was necessary to prepare test samples in parallel, resulting in different surface properties compared to samples of IFAM preparations (see Table 3). This adds uncertainties to the result interpretation. However, CRREL used the same PTFE tape material (3M tape 5490) as IFAM for the sample preparations. This allowed for the best comparability in this study, and results for the mechanical tests indicated the following result ranking: 323 kPa (INTA) > 189 kPa (NTNU) > 158 kPa (ND) > 102 kPa (CRREL) > 71 kPa (RISE). For the CRREL tension test, the data were the lowest (32 kPa) in this study. In this configuration, the ice was lifted directly off the surface with minimal sliding or shear components along the interface. Unlike shear delamination modes, tensile delamination involves minimal interfacial sliding friction between the ice and substrate materials during delamination. As a result, different forces govern delamination in tension vs. shear modes, and different relative rankings can be expected.

A detailed assessment of test parameter dependencies provided additional findings:

- The standard deviations showed that there is good agreement between RSE and INTA results. For both tests, ice formations were conducted overnight. For the other round-robin tests, icing times between 35 min and 180 min were used (see Table 5). Additionally, the test samples were completely embedded in the ice compound for the RSE and INTA tests instead of only one flat homogeneous surface that was covered by ice (see Table 4). These differences might have led to increased ice adhesion results, especially for PUR C25 and PTFE tape, compared with the remaining shear test results.
- The deviation in the ice formation temperature for RSE (−19 °C instead of the harmonized −8 °C for the rest of the test program, Table 5) did not seem to affect the results significantly.

No correlations could be observed amongst the mechanical tests between ice adhesion results and area of ice coverage, displacement type (push/pull), and displacement speed.

3.2. Centrifuge Tests (NU, IFAM, AMIL, TAU, and P-A)

Centrifuge tests were conducted by five contributors using different types of ice. The results are summarized in Figure 8. The figure includes results for static and impact ice formations, the latter accreted in ice wind tunnels with wind speeds as indicated. Mean and standard deviations are shown; these are derived from raw data displayed in Appendix A —Table A2.

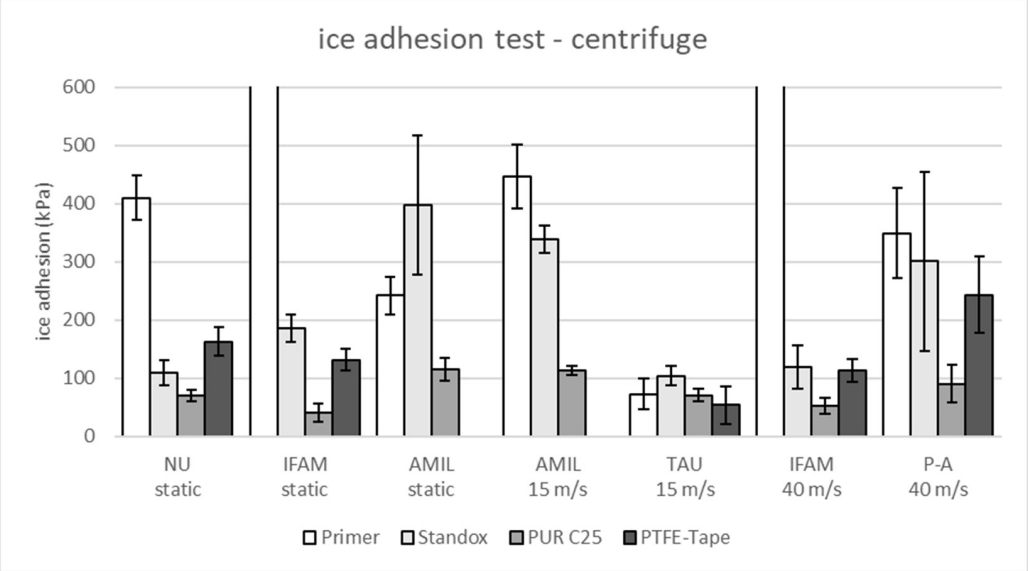

Figure 8. Results for centrifuge ice adhesion tests. Bars exceeding the ice adhesion axis refer to the qualitative result: high ice adhesion strength, resulting in cohesive ice failure.

Results for static ice formations were delivered by three partners. The PUR C25 material showed the lowest ice adhesion strength data for the materials in testing, with 116 kPa (AMIL), 70 kPa (NU), and 41 kPa (IFAM). For the Primer and Standox materials, no consistent material ranking trend could be observed.

For impact ice, accreted at a wind speed of 15 m/s, no consistent material ranking was observed for the two delivering partners AMIL and TAU. This may be linked to deviations in ice conditioning times, with 17 h for the TAU facility and 10 min for the AMIL facility. For partners IFAM and P-A (impact ice, 40 m/s), the following material ranking was identified: Primer ≥ Standox ≥ PTFE tape > PUR C25.

A direct comparison of different ice types can be conducted for test results from AMIL and IFAM. AMIL tested ice adhesion using static ice as well as impact ice accreted at 15 m/s. For the PUR C25 and Standox materials, no significant differences in ice adhesion strength data amongst the ice types were observed. For the Primer material, the ice adhesion strength for static ice was significantly lower (242 kPa) compared to that of impact ice (446 kPa).

It can be postulated that the high surface roughness of the coating causes a mechanical interlocking of ice due to the impinging of water droplets under freezing conditions. A similar finding has been reported for an aluminum surface [50].

IFAM observed cohesive ice failure for Primer coating (qualitative result), regardless of the ice type. For the PTFE tape and PUR C25 materials, no significant differences between the ice types were observed. A quantifiable deviation was observed for the Standox coating, with 118 kPa for impact ice (40 m/s) and 185 kPa for static ice. This is not in accordance with the findings for the Primer coating in AMIL tests. Standox and Primer surfaces showed different surface roughness. The effects of the difference in surface roughness on the results of different ice types remain unclear and underline the need for systematic assessments considering various ice types in the material evaluations.

For further parameter assessment, tests were grouped into the ice types "static" and "impact". For tests using static ice, the iced areas and ice masses increased amongst the test designs as follows: NU (1.38 cm^2; 1.3 g) < IFAM (9 cm^2; 3 g) < AMIL (11.2 cm^2; 7 g). No potential correlations were observed in the measurement data for PUR C25, but for the Standox coating, increasing ice adhesion strength was observed for higher ice masses.

Additionally, the shear stress evolution during the centrifuge tests differed significantly in this study and resulted in the same ranking as that for the ice masses: NU << IFAM < AMIL (see Figure 9). The lower the centrifuge acceleration speed, the higher the resolution for the low ice adhesion region (e.g., < 100 kPa) and the higher the cumulative stresses over the test duration. The observed low ice adhesion strength for Standox coating in NU tests (109 kPa)—the lowest acceleration speed in this study—could be linked to an increased test duration/cumulative stress. An increased acceleration speed (shorter test times) may then lead to increased ice adhesion strength data for tests at IFAM (185 kPa) and AMIL (397 kPa). However, for the PUR C25 and PTFE tape materials with expected low ice adhesion, this effect was not observed.

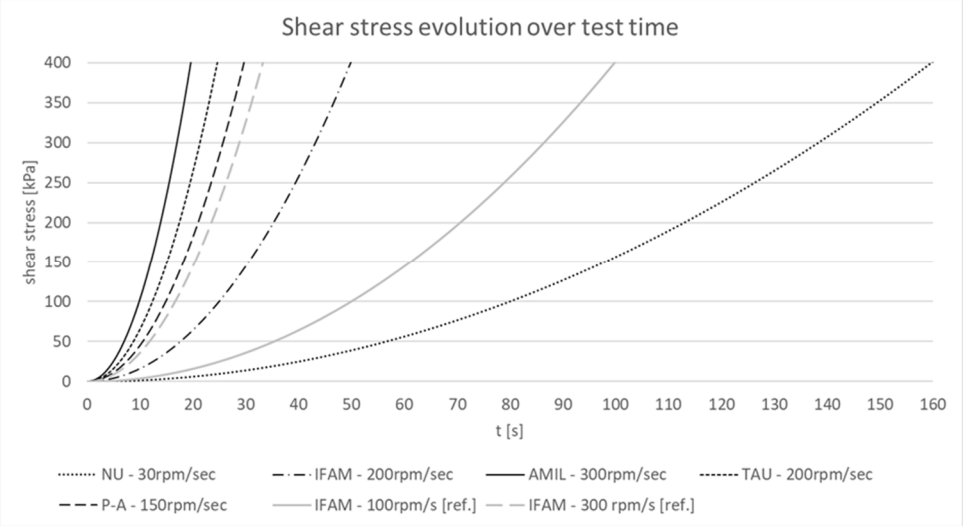

Figure 9. Shear stress evolution for centrifuge tests in this study. Graphs (IFAM—100 rpm/s, IFAM—300 rpm/s (in grey)) were adapted from [31].

In a parallel IFAM study with increasing acceleration speeds of 100 rpm/s, 200 rpm/s, and 300 rpm/s and a fixed ice mass of 3 g, a slight increase in the ice adhesion strength was observed for the highest acceleration speed in the test (Standox: 185 kPa, 185 kPa, and 217 kPa) [31]. However, the observed difference was not significant considering the standard deviations, and factual correlations remain unclear due to the observed multiparameter dependency.

For impact ice adhesion tests, the four test designs in this study used comparable ice areas (9 cm^2 to 11.2 cm^2), but the ice masses differed significantly with IFAM~3 g << AMIL~7 g < TAU~8 g < P-A~9 g (see Table 6). These results were accompanied by

increasing ice thickness and different ice shapes for the tests. However, correlations with ice adhesion test data were not observed for any of the tested materials. This also applies to the parameter shear stress evolution, which was lowest for IFAM (200 rpm/s), followed by P-A, TAU, and AMIL in a narrow range. The high complexity of parameter setups prevents the clear identification of dependencies, which remains an open topic in this study.

3.3. Mode I Tests (CU, ConU)

Mode I tests were conducted by two partners in this study. Impact ice was used, and test parameters were harmonized between the facilities (see Table 6). The results, including means and standard deviations, are summarized in Figure 10 for the four test surfaces; these results are based on the raw data included in Appendix A—Table A3.

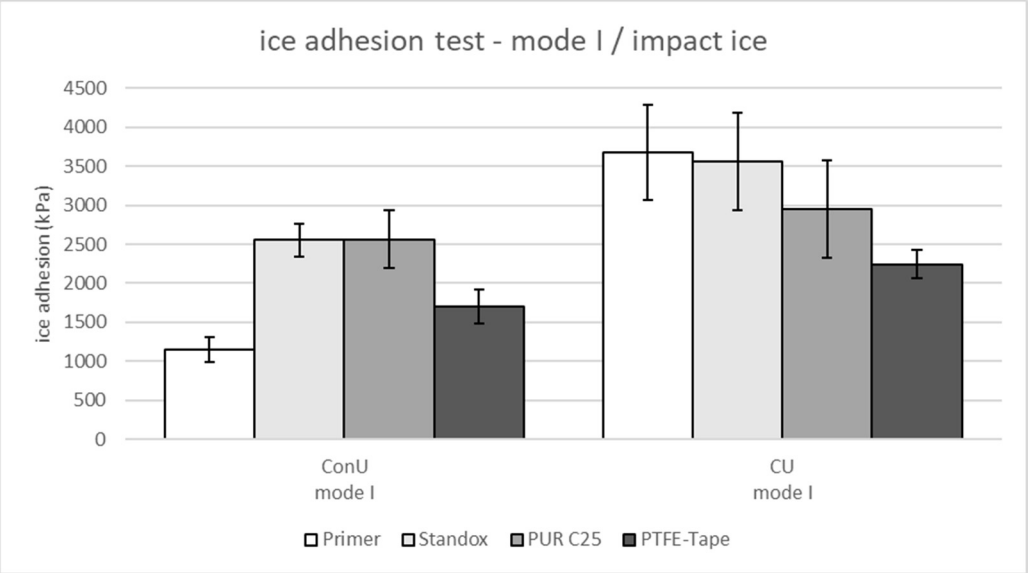

Figure 10. Results for Mode I ice adhesion tests.

The ranking for the test surfaces differed between the partners. The most significant difference was found for the Primer coating. The best agreement could be observed for the PTFE tape material.

The remaining parameter difference between the facilities after the harmonization process was the iced area; this measured 7.07 cm^2 for CU and 12.6 cm^2 for ConU (assuming that the ice masses are comparable). The calculated ice volumes were ~11 cm^3 for CU and ~12 cm^3 for ConU. In this study, the impact of the test parameter on the ice adhesion test results was unclear.

4. Discussion

This study aimed to compare ice adhesion test results using identical test surfaces but different test designs at 13 partner facilities. In the definition phase, the homogenization of test parameters was conducted, and test designs were grouped according to the ice types and ice removal techniques used. Table 7 summarizes the results and provides a material ranking based on the absolute values for the averaged ice adhesion strength data.

Table 7. Summary of ice adhesion test results in this study, including a material ranking for increasing means of ice adhesion strength, with cells colored in white < light grey < dark grey < black.

TYPE	Test Facility	Test Name	Sample Geometry	Ice Type	Ice Adhesion [kPa] Mean (stdev)				Difference from General Test Program
					Primer	Standox	PUR C25	PTFE Tape	
PULL	RSE	Shear: pull	Cylindrical	Static	544 (71)	700 (62)	274 (100)	No data	Ice formation at −19 °C overnight
	INTA	Double-lap shear	Flat	Static	554 (83)	472 (195)	326 (99)	323 (51)	Overnight
PUSH	NTNU	Ice shear test	Flat	Static	195 (14)	274 (39)	141 (28)	189 (47)	
	RISE	Shear: push	Flat	Static	cohesive	351 (39)	63 (19)	71 (44)	
	ND	Shear: push	Flat	Static	228 (23)	297 (12)	78 (6)	158 (12)	
	CRREL	Peel test (shear)	Flat	Static	133 (9)	117 (7)	No data	102 (8)	
TENSION	CRREL	Peel test (tension)	Flat	Static	26 (2)	19 (1)	No data	32 (1)	Sample preparation at CRREL
CENTRIFUGE	AMIL	Centrifuge	Flat	Static	242 (33)	397 (119)	116 (20)	No data	
	IFAM	Centrifuge	Flat	Static	cohesive	185 (24)	41 (15)	131 (18)	
	NU	Centrifuge	Flat	Static	409 (38)	109 (21)	70 (10)	163 (25)	
CENTRIFUGE	AMIL	Centrifuge	Flat	Impact 15 m/s	446 (54)	339 (24)	113 (8)	No data	
	TAU	Centrifuge	Flat	Impact 15 m/s	73 (27)	104 (17)	98 (56)	54 (32)	
	IFAM	Centrifuge	Flat	Impact 40 m/s	cohesive	118 (37)	52 (14)	112 (20)	
	Partner P-A	Centrifuge	Cylindrical	Impact 40 m/s	349 (77)	301 (154)	90 (33)	243 (66)	
MODE I	ConU	Mode I	Cylinder end	Impact 40 m/s	1154 (157)	2555 (210)	2564 (375)	1701 (216)	
	CU	Mode I	Cylinder end	Impact 40 m/s	3675 (615)	3563 (622)	2955 (625)	2242 (184)	

The Primer (high roughness and hydrophilic) and Standox (low roughness and hydrophilic) materials were expected to show higher ice adhesion test results compared to the PUR C25 (low roughness and hydrophobic) and the PTFE tape (high roughness and hydrophobic). The results from each partner facility were mainly in accordance with these expectations. However, the absolute values among the facilities differ significantly and do not allow for a general definition of a specific value for low ice adhesion surfaces.

For the mechanical tests, it was observed that icing times and/or geometries of the ice/test surface interface have significant effects on ice adhesion strength. The longer icing times (overnight) as well as the complete immersion of the test samples during the icing process in INTA and RSE tests led to higher shear forces, especially for PUR C25 and PTFE tape. For the remaining mechanical tests, reasonable comparability in ice adhesion strength data was identified between pull-based (RISE) and push-based (NTNU, ND, and CRREL) tests.

For the centrifuge tests in this study, the direct comparison of static and impact ice in tests at AMIL and IFAM did not show differences for the potential low ice adhesion surfaces. The comparison of all centrifuge test designs showed the most obvious differences for the ice-covered area, the ice mass and shape, and the evolution of the shear stress. These parameters may have contrary effects on the measurement data, preventing the identification of correlations between test parameters and ice adhesion strength results. Further systematic studies would improve our understanding of the most decisive test parameter.

The result comparison for mechanical shear tests and centrifuge tests with comparable ice preparation times (from 10 min for impact ice to 200 min for static ice) shows, for the PUR C25, a comparably narrow range of mean data: from a minimum of 41 kPa (IFAM centrifuge using static ice) to a maximum of 141 kPa (NTNU push-based test using static ice). For PTFE tape, the range of measurement data increased from 71 kPa (RISE pull-based

test using static ice) to 243 kPa (P-A centrifuge test using impact ice). For the materials for which a high ice adhesion strength was expected (Standox and Primer), the result ranges increased further, also indicating a potential risk for false positive (low) ice adhesion evaluations. However, the available results provided no indications about how to mitigate these risks regarding a specific test design. For surface evaluations, it is thus recommended to perform different test methods, rather than focusing on one test, to reduce uncertainties.

The Mode I tests in this study showed significantly higher ice adhesion strength values. The test designs differed significantly from the mechanical and centrifuge tests. Failure types (tension vs. shear) and other differences were discussed. During the ice adhesion measurements for the Mode I tests, the respective ice wind tunnel, including the water spray system, was active. This is of high relevance for actual technical applications and may have led to completely different data, but our understanding of its relevance to the assessment of low ice adhesion surfaces needs to be improved.

The use of absolute ice adhesion values is discussed in the literature because of the uneven force distribution for most of the test designs, e.g., in [5,42]. Amongst others, this resulted in the introduction of the adhesion reduction factor (ARF) to set the values in relation to a benchmark material [13]. In this study, for each test method, the Standox material (as unmodified PUR material) was defined as the test-specific reference material. Regarding the ice adhesion value, the percentage of reduction was calculated for PUR C25 (Figure 11) and PTFE tape (Figure 12).

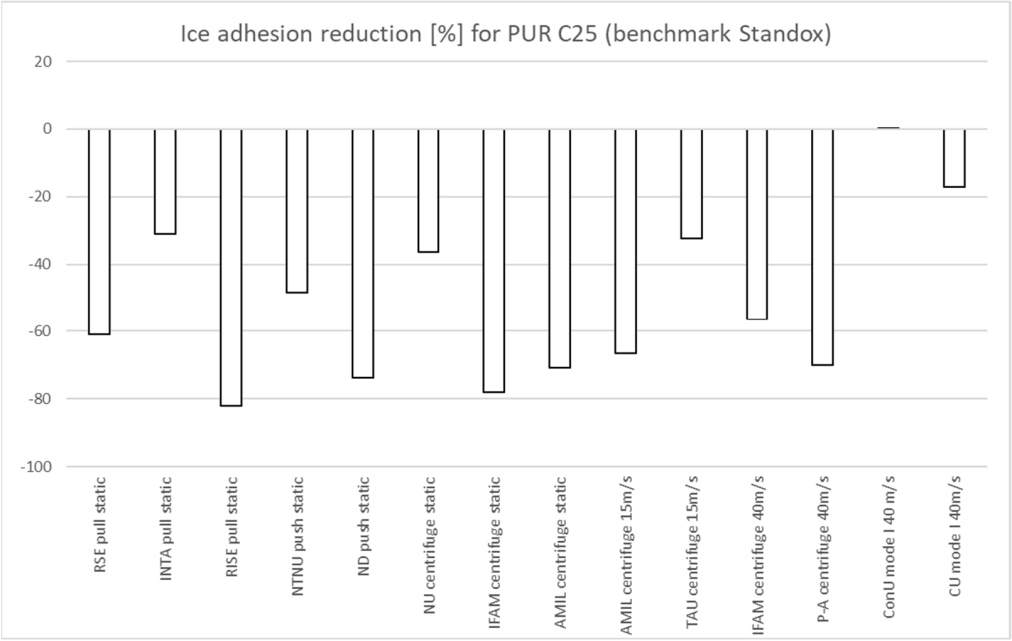

Figure 11. Ice adhesion reduction (%) for each test in this study, based on the test-specific results for Standox (reference) and PUR C25.

In this study, the percental reduction for PUR C25 ranged from 0% for ConU to −82% for RISE. No basic trend could be observed for ice types or test designs. The same trend was observed for the PTFE tape results, for which the resulting span was even larger compared to the respective Standox reference material: from +72% for the CRREL tension test to −80% for the RISE push test. CRREL prepared test samples in parallel to the IFAM preparations. Despite the highest possible diligence in the processes, differences in surface properties occurred, which affected the ice adhesion test results, thus highlighting the necessity of single-source surface preparations for comparison tests.

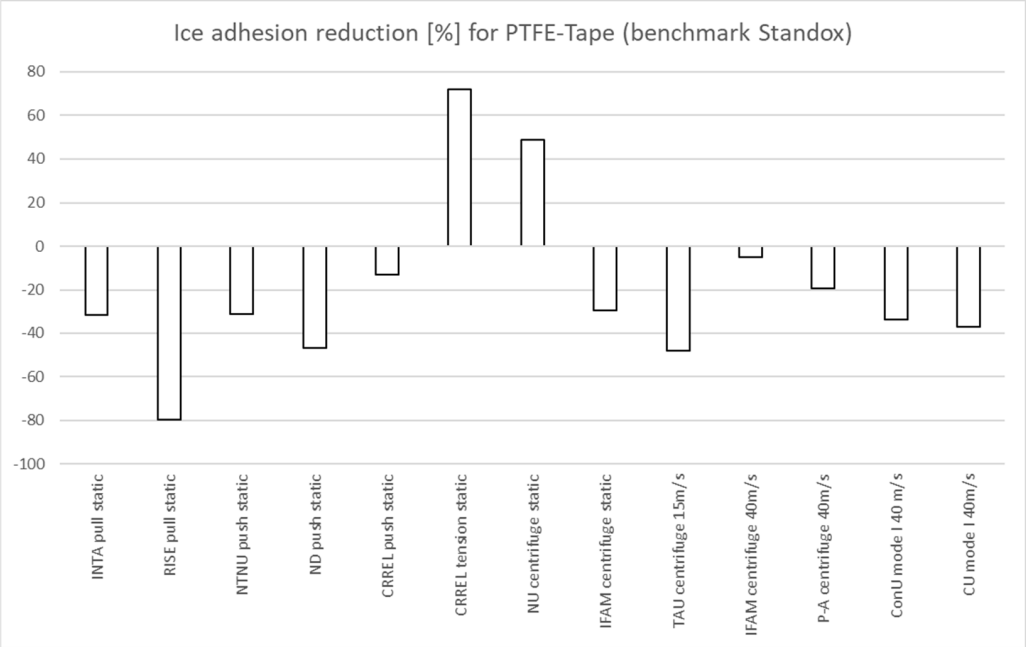

Figure 12. Ice adhesion reduction (%) for each test in this study, based on the test-specific results for Standox (reference) and PTFE tape.

In conclusion, this study highlights the extreme difficulty of comparing ice adhesion measurements not only among different methodologies, but also within the same measurement techniques. A harmonization of parameters, especially from the method of ice formation on the test surface, and an optimization of measurement parameters to lower the standard deviation should be performed in order to produce data that are more comparable among laboratories. Based on the results of this study, it is unlikely that a unified test standard for ice adhesion measurements can be developed. Future topics should address the identification of the most relevant test parameters and work on correction factors in the dependence of ice adhesion measurement techniques, preferably supported by data from relevant technical applications for icephobic materials. In addition, test conditions should be selected to be as similar to application conditions as possible.

Author Contributions: Conceptualization, N.R. and V.S.; Data curation, N.R.; Investigation, N.R., J.-D.B., M.Y., M.B., H.K., J.M., J.H., M.-L.P., A.D., E.A.-S., M.J. and X.H.; Methodology, N.R.; Project administration, N.R.; Resources, N.R. and E.A.-S.; Supervision, V.S.; Validation, J.-D.B., H.S., M.B., H.K., J.M., J.H., M.-L.P., A.D., E.A.-S., M.J., X.H. and V.S.; Visualization, N.R.; Writing—original draft, N.R., J.-D.B., M.Y., H.K., J.M., J.H., M.-L.P., A.D., E.A.-S., M.J. and X.H.; Writing—review and editing, H.S., M.B. and V.S. All authors have read and agreed to the published version of the manuscript.

Funding: The RSE activity has been financed by the Research Fund for the Italian Electrical System under the Three-Year Research Plan 2022–2024 (DM MITE n. 337, 15.09.2022), in compliance with the Decree of 16 April 2018. Further contributors to this research received no external funding.

Data Availability Statement: The data presented in this study are available in Appendix A of this manuscript.

Acknowledgments: The authors would like to thank their organizations and institutions for providing the test infrastructure and supporting this activity. We thank the Fraunhofer IFAM for the financial support to prepare and deliver the test specimen to the contributing partners.

Conflicts of Interest: The authors declare no conflicts of interest.

Appendix A

Table A1. Raw data [kPa] from ice adhesion tests—direct mechanical tests.

Contributor	**RSE**						**INTA**						**RISE**				**NTNU**				**NotreDame**						**CRREL**			**CRREL**	
Test Type	**Pull-Out/Static Temperature (Ice Formation −19 °C)**						**Pull/Static**						**Pull/Static**				**Push/Static**				**Push/Static**						**Push/Static**			**Tension/Static**	
Material	**#**	**Run 1**	**#**	**Run 1**	**Mean**	**Stdev**	**#**	**Run 1**	**Run 2**	**Run 3**	**Mean**	**Stdev**	**#**	**Run 1**	**Mean**	**Stdev**	**#**	**Run 1**	**Mean**	**Stdev**	**#**	**Run 1**	**Run 2**	**Run 3**	**Mean**	**Stdev**	**#**	**Mean**	**Stdev**	**#**	**Mean**	**Stdev**
Primer	1	586	11	577			1	621	579	426			1	coh				203				207	225	252								
	2	561	12	490			2	668	500	574			2	coh				204														
	3	510	13	624			3	705	495	584			3	coh				179														
	4	553	14	402			4	484	479	537			4	coh																		
	5	489	15	532																												
	6	436	16	606																												
	7	594	17	677																												
	8	504	18	no data																												
	9	593	19	600																												
	10	562	20	438	544	71					554	83			coh				195	14					228	23		133	9		26	2
Standox	21	601	26	814			8	148	447	589			8	301				308				288	292	310								
	22	no data	27	663			9	163	437	647			9	343				232														
	23	688	28	667			10	300	568	768			#	369				282														
	24	693	29	678			11	395	647	553			#	390																		
	25	751	30	747	700	62					472	195			351	39			274	39					297	12		117	7		19	1
PUR C25	31	158	36	401			12	258	442	442			#	86				171				72	79	83								
	32	270	37	100			13	268	332	453			#	42				114														
	33	291	38	290			14	211	305	321			#	71				139														
	34	194	39	301			15	142	321	416			#	52																		
	35	317	40	415	274	100					326	99			63	19			141	28					78	6		no data	no data		no data	no data
PTFE-Tape	no data						5	337	326	384			5	81				154				155	148	171								
							6	311	232	353			6	109				170														
					no data	no data	7	258	321	384	323	51	7	23	71	44		242	189	47					158	12		102	8		32	1
	Q-test analysis with aberrant 99%														coh = cohesive failure																

Table A2. Raw data [kPa] from ice adhesion tests—centrifuge test.

Contributor		Nottingham University				IFAM										AMIL						AMIL						TAU						IFAM										P-A					
Test Type		Centrifuge/Static				Centrifuge/Static										Centrifuge/Static						Centrifuge/15 m/s						Centrifuge/15 m/s						Centrifuge/40 m/s										Centrifuge/40 m/s A = Aluminum; C = Composite					
Material	#	Run 1	Run 2	Mean	Stdev	#	Run 1	Run 2	Run 3	Run 4	Run 5	Run 6	Run 7	Mean	Stdev	#	Run 1	Run 2	Run 3	Mean	Stdev	#	Run 1	Run 2	Run 3	Mean	Stdev	#	Run 1	Mean	Stdev	#	Run 1	Run 2	Run 3	Run 4	Run 5	Run 6	Run 7	Run 8	Mean	Stdev	#	Run 1	Run 2	Run 3	Mean	Stdev
Primer	1	397	378			Z1	coh	coh	coh							AMIL1	236	234	274			AMIL1	411	499	525			1	76			Z1	coh	coh	coh							A3	358	no data	290	A:	
	2	469	410			Z2	coh	coh	coh							AMIL2	225	284	196			AMIL2	434	386	421			2	56			Z2	coh	coh	coh							A4	287	396	256	317	58
	3	397	372			Z3	coh	coh	coh																			3	110			Z3	coh	coh	coh							C2	411	299	237		
	4	416	345																									4	49													C3	366	438	no data	C:	
	5	410	416																																							C10	290	480	425	368	85
	6	384	497																																											
	7	410	429	409	38									coh						242	33					446	54			73	27									coh				A+C:	349	77
Standox	13	106	148			Z9	218									AMIL3	303	397	551			AMIL3	298	327	363			8	117			Z11	111	157								C6	76	205	no data		
	14	70	106			Z10	148									AMIL4	472	220	440			AMIL4	343	341	360			9	85			Z13	181	116	64	118						C7	197	335	475		
	15	119	109			Z11	204	165																				11	109			A1	64	144								C11	194	475	447		
	16	96	133			Z13	165	203																								A3	100	128												
	17	102	106			A1	189																																								
				109	21	A2	191							185	24					397	119					339	24			104	17									118	37				301	154
PUR C25	18	55	58			Z14	28	29	59							AMIL5	132	131	107			AMIL5	122	104	122			12	82			Z14	50	54	58	32	43					A1	114	129	161	A:	
	19	78	63			Z15	29									AMIL6	131	110	82			AMIL6	107	109	115			13	61			Z15	51	82	48							A2	36	94	128	110	43
	20	73	63			Z17	24	32	72	45	39	37																14	no data			Z18	39	58								C1	117	79	74		
	21	70	78			Z18	61	17	29	55																		15	67														C4	72	74	64	C:	
	22	73	87			B2	52	40																																		C5	54	85	75	77	17
				70	10									41	15					116	20					113	8			70	11									52	14			A+C:	90	33
PTFE-Tape	8	164	148			Z5	160	123								no data						no data						5	38			Z5	131	89								C8	no data	278	258		
	9	168	181			Z6	143	147	124	129	158	144	111															6	32			Z6	133	122								C9	no data	282	281		
	10	119	189			Z7	105	105	129																			7	91			Z8	94	110	141	103	95	80	121	128		C12	104	281	215		
	11	144	207			Z8	150	122	118																																						
	12	160	148	163	25									131	18					no data						no data		54	32									112	20				243	66

Ice shed may have been caused by impact of ice from adjacent sample

Table A3. Raw data [kPa] from ice adhesion tests—Mode I tests.

Contributor		Concordia University Mode I/Impact 40 m/s						Cranfield Univ. Mode I/Impact 40 m/s						
Test Type														
Material	#	Run 1	Run 2	Run 3	Mean	Stdev	#	Run 1	Run 2	Run 3	Run 4	Run 5	Mean	Stdev
Primer	1	1037	1358	1124			1	coh	2740	3770	3500	3880		
	2	1142	961	1427			2	coh	3530	4630	coh	coh		
	3	1236	1064	1034	1154	157							3675	615
PTFE-Tape	4	1700	1558	1635			4	1990	2080	2240	2500	2320		
	5	1874	1765	1422			5	2320						
	6	1524	1678	2153	1701	216							2242	184
Standox	7	2336	2829	2193			7	3430	3120	4130	2780	3530		
	8	2682	2500	2524			8	5000	3170	3670	3560	3250		
	9	2831	2524	2575	2555	210							3564	622
PUR C25	10	2071	2794	2427			10	3960	2280	2310	2630	2380		
	11	2211	2739	2689			11	3630	2880	2640	3100	3740		
	12	2818	3192	2137	2564	375							2955	625

References

1. Antonini, C.; Innocenti, M.; Horn, T.; Marengo, M.; Amirfazli, A. Understanding the Effect of Superhydrophobic Coatings on Energy Reduction in Anti-Icing Systems. *Cold Reg. Sci. Technol.* **2011**, *67*, 58–67. [CrossRef]
2. Kulinich, S.A.; Farhadi, S.; Nose, K.; Du, X.W. Superhydrophobic Surfaces: Are They Really Ice-Repellent? *Langmuir* **2011**, *27*, 25–29. [CrossRef] [PubMed]
3. Kreder, M.J.; Alvarenga, J.; Kim, P.; Aizenberg, J. Design of Anti-Icing Surfaces: Smooth, Textured or Slippery? *Nat. Rev. Mater.* **2016**, *1*, 15003. [CrossRef]
4. Golovin, K.; Kobaku, S.P.R.; Lee, D.H.; Di Loreto, E.T.; Mabry, J.M.; Tuteja, A. Designing Durable Icephobic Sur-faces. *Sci. Adv.* **2016**, *2*, e1501496. [CrossRef] [PubMed]
5. Wohl, C.J.; Berry, D.H. *Contamination Mitigating Polymeric Coatings for Extreme Environments*; Wohl, C.J., Berry, D.H., Eds.; Part II: Ice Contamination-Mitigating Coatings; Advances in Polymer Science 284; Springer Nature: Cham, Switzerland, 2019; pp. 52–214.
6. Asadollahi, S.; Farzaneh, M.; Stafford, L. On the icephobic behavior of organosilicon-based surface structures de-veloped through atmospheric pressure plasma deposition in nitrogen plasma. *Coatings* **2019**, *9*, 679. [CrossRef]
7. Huang, X.; Tepylo, N.; Pommier-Budinger, V.; Budinger, M.; Bonaccurso, E.; Villedieu, P.; Bennani, L. A survey of icephobic coatings and their potential use in a hybrid coating/active ice protection system for aerospace applications. *Prog. Aerosp. Sci.* **2019**, *105*, 74–97. [CrossRef]
8. Liu, G.; Yuan, Y.; Liao, R.; Wang, L.; Gao, X. Fabrication of a porous slippery icephobic surface and effect of lubri-cant viscosity on anti-icing properties and durability. *Coatings* **2020**, *10*, 896. [CrossRef]
9. Esmeryan, K.D. From ExtremelyWater-Repellent Coatings to Passive Icing Protection—Principles, Limitations and Innovative Application Aspects. *Coatings* **2020**, *10*, 66. [CrossRef]
10. Milles, S.; Vercillo, V.; Alamri, S.; Aguilar-Morales, A.I.; Kunze, T.; Bonaccurso, E.; Lasagni, A.F. Icephobic per-formance of multi-scale laser-textured aluminum surfaces for aeronautic applications. *Nanomaterials* **2021**, *11*, 135. [CrossRef]
11. Parent, O.; Ilinca, A. Anti-icing and De-icing Techniques for Wind Turbines: Creitical Review. *Cold Reg. Sci. Technol.* **2021**, *65*, 88–96. [CrossRef]
12. Mora, J.; García, P.; Carreño, F.; González, M.; Gutiérrez, M.; Montes, L.; Agüero, A. Setting a comprehen-sive strategy to face the runback icing phenomena. *Surf. Coat. Technol.* **2023**, *465*, 129585. [CrossRef]
13. Laforte, C.; Beisswenger, A. Icephobic Material Centrifuge Adhesion Test. In Proceedings of the IWAIS 2005, Montréal, QC, Canada, 12–16 June 2005.
14. Arianpoura, F.; Farzaneh, M.; Kulinich, S.A. Hydrophobic and ice-retarding properties of doped silicone rubber coatings. *Appl. Surf. Sci.* **2013**, *265*, 546–552. [CrossRef]
15. Soltis, J.; Palacios, J.; Eden, T.; Wolfe, D. Evaluation of Ice-Adhesion Strength on Erosion-Resistant Materials. *AI-AA J.* **2015**, *53*, 1825–1835. [CrossRef]
16. Janjua, Z.A.; Turnbull, B.; Choy, K.-L.; Pandis, C.; Liu, J.; Hou, X.; Choia, K.-S. Performance and Durability Tests of Smart Icephobic Coatings to Reduce Ice Adhesion. *Appl. Surf. Sci.* **2017**, *407*, 555–564. [CrossRef]
17. Orchard, D.; Clark, C.; Chevrette, G. Reducing Aviation Icing Risk: Ice Adhesion Measurement in the NRC's Altitude Icing Wind Tunnel. In Proceedings of the SAE AeroTech Conference, FortWorth, TX, USA, 26–28 September 2017.
18. Rønneberg, S.; Laforte, C.; Volat, C.; He, J.; Zhang, Z. The effect of ice type on ice adhesion. *AIP Adv.* **2019**, *9*, 055304. [CrossRef]
19. Brassard, J.D.; Laforte, C.; Guerin, F.; Blackburn, C. Icephobicity: Definition and Measurement Regarding Atmos-pheric Icing. In *Contamination Mitigating Polymeric Coatings for Extreme Environments*; Wohl, C.J., Berry, D.H., Eds.; Springer International Publishing: Cham, Switzerland, 2019; pp. 123–144. [CrossRef]
20. Tetteh, E.; Loth, E. Reducing Static and Impact Ice Adhesion with a Self-Lubricating Icephobic Coating (SLIC). *Coatings* **2020**, *10*, 262. [CrossRef]
21. Schulz, M.; Sinapius, M. *Evaluation of Different Ice Adhesion Tests for Mechanical Deicing Systems*; SAE Technical Paper 2015-01-2135; SAE International in United States: Warrendale, PA, USA, 2015. [CrossRef]

22. Work, A.; Lian, Y. A Critical Review of the Measurement of Ice Adhesion to Solid Substrates. *Prog. Aerosp. Sci.* **2018**, *98*, 1–26. [CrossRef]
23. Rønneberg, S.; He, J.; Zhang, Z. The need for standards in low ice adhesion surface research: A critical review. *J. Adhes. Sci. Technol.* **2020**, *34*, 319–347. [CrossRef]
24. Emelyanenko, K.A.; Emelyanenko, A.M.; Boinovich, L.B. Water and ice adhesion to solid surfaces: Common and specific, the impact of temperature and surface wettability. *Coatings* **2020**, *10*, 648. [CrossRef]
25. Nazifi, S.; Firuznia, R.; Huang, Z.; Jahanbakhsh, A.; Ghasemi, H. Predicitve model of ice adhesion on non-elastomeric materials. *J. Colloid Interface Sci.* **2023**, *648*, 481–487. [CrossRef] [PubMed]
26. Stendardo, L.; Gastaldo, G.; Budinger, M.; Pommier-Budinger, V.; Tagliaro, I.; Ibánez-Ibánez, P.F.; Antonini, C. Reframing ice adhesion mechanisms on a solid surface. *Appl. Surf. Sci.* **2023**, *641*, 158462. [CrossRef]
27. Nistal, A.; Sierra-Martín, B.; Fernández-Barbero, A. On the Durability of Icephobic Coatings: A Review. *Materials* **2024**, *17*, 235. [CrossRef] [PubMed]
28. Hejazi, V.; Sobolev, K.; Nosonovsky, M. From superhydrophobicity to icephobicity: Forces and interaction analysis. *Sci. Rep.* **2013**, *3*, 2194. [CrossRef] [PubMed]
29. Dou, R.; Chen, J.; Zhang, Y.; Wang, X.; Cui, D.; Song, Y.; Jiang, L.; Wang, J. Anti-icing coating with an aqueous lubri-cating layer. *ACS Appl. Mater. Interfaces* **2014**, *6*, 6998–7003. [CrossRef]
30. Makkonen, L. Ice Adhesion—Theory, Measurements and Countermeasures. *J. Adhes. Sci. Technol.* **2012**, *26*, 413–445. [CrossRef]
31. Rehfeld, N.; Speckmann, B.; Stenzel, V. Parameter Study for the Ice Adhesion Centrifuge Test. *Appl. Sci.* **2022**, *12*, 1583. [CrossRef]
32. *DIN EN ISO 2808:2019*; Beschichtungsstoffe—Bestimmung der Schichtdicke. Beuth Verlag GmbH: Berlin, Germany, 2019.
33. Rehfeld, N.; Speckmann, B.; Schreiner, C.; Stenzel, V. Assessment of Icephobic Coatings—How Can We Monitor Performance Durability? *Coatings* **2021**, *11*, 614. [CrossRef]
34. *DIN EN ISO 19403-2*; Beschichtungsstoffe—Benetzbarkeit—Teil 2: Bestimmung der freien Oberflächenenergie fester Ober-flächen durch Messung des Kontaktwinkels. Beuth Verlag GmbH: Berlin, Germany, 2020.
35. *DIN EN ISO 19403-7*; Beschichtungsstoffe—Benetzbarkeit—Teil 7: Messung des Kontaktwinkels bei Neigetisch-Experimenten (Abrollwinkel). Beuth Verlag GmbH: Berlin, Germany, 2020.
36. Balordi, M.; Cammi, A.; Santucci de Magistris, G.; Chemelli, C. Role of micrometric roughness on anti-ice proper-ties and durability of hierarchical super-hydrophobic aluminum surfaces. *Surf. Coat. Technol.* **2019**, *374*, 549–556. [CrossRef]
37. Ferrick, M.G.; Mulherin, N.D.; Haehnel, R.B.; Coutermarsh, B.A.; Durell, G.D.; Tantillo, T.J.; Welser, E.S.; Cano, R.J.; Smith, R.J.; Martinez, E.C. *Double Lap Shear Testing of Coating Modified Ice Adhesion to Liquid Oxygen Food Line Bracket, Space Shuttle External Tank*; No. ERDC/CRREL-TR-06-11; Engineering Research and Development Center Hanover nh Cold Regions Research and Engineering Lab: Hanover, NH, USA, 2006.
38. Chernyy, S.; Järn, M.; Shimizu, K.; Swerin, A.; Pedersen, S.U.; Daasbjerg, K.; Makkonen, L.; Claesson, P.; Irutha-yaraj, J. Superhydrophilic Polyelectrolyte Brush Layers with Imparted Anti-Icing Properties: Effect of Counter ions. *ACS Appl. Mater. Interfaces* **2014**, *6*, 6487–6496. [CrossRef]
39. Asenath-Smith, E.; Hoch, G.R.; Erb, C.T. Adhesion of freshwater columnar ice to material surfaces by crystallization from the melt. *J. Cryst. Growth* **2020**, *535*, 125563. [CrossRef]
40. Lovell, A.R.; Hoch, G.R.; Donnelly, C.J.; Hodge, J.M.; Haehnel, R.B.; Asenath-Smith, E. Shear and Tensile Delamination of Ice From Surface: The Ice Ahdesion Peel Test (IAPT). ERDC/CRREL Tech. Note, TN-21-1; U.S. Army Engineer Research and Development Center, Cold Regions Research and Engineering Laboratory, USA. 2021. Available online: https://apps.dtic.mil/sti/trecms/pdf/AD1147237.pdf (accessed on 13 January 2024).
41. *ISO/TS 19392-6:2023 (E)*; Paints and Varnishes—Coating Systems for Wind-Turbine Rotor Blades—Part 6: Determination and Evaluation of Ice Adhesion Using Centrifuge. ISO: Geneva, Switzerland, 2023.
42. Memon, H.; De Focatiis, D.S.A.; Choi, K.-S.; Hou, X. Durability enhancement of low ice adhesion polymeric coat-ings. *Prog. Org. Coat.* **2021**, *151*, 106033. [CrossRef]
43. Koivuluoto, H.; Hartikainen, E.; Niemelä-Anttonen, H. Thermally Sprayed Coatings: Novel Surface Engineering Strategy towards Icephobic Solutions. *Materials* **2020**, *13*, 1434. [CrossRef] [PubMed]
44. Niemelä-Anttonen, H.; Kiilakoski, J.; Vuoristo, P.; Koivuluoto, H. Icephobic Performance of Different Surface Designs and Materials. In Proceedings of the International Workshop on Atmospheric Icing of Structures, IWAIS2019, Reykjavik, Iceland, 23–28 June 2019; p. 5.
45. Hammond, D.; Luxford, G.; Ivey, P. The Cranfield University Icing Tunnel. In Proceedings of the 41st Aerospace Sciences Meeting and Exhibit, Reno, NV, USA, 6–9 January 2003; AIAA 2003-901. Available online: https://arc.aiaa.org/doi/pdf/10.2514/6.2003-901 (accessed on 13 January 2024).
46. Grasso, M.J. Development of a Mode I Test Rig for Quantitative Measurements of Ice Adhesion Using Tensile Stress. Master's Thesis, Concordia University, Montreal, QC, Canada, 2019.
47. Andrews, E.H.; Stevenson, A. Fracture energy of epoxy resin under plane strain conditions. *J. Mater. Sci.* **1978**, *13*, 1680–1688. [CrossRef]
48. Andrews, E.H.; Lockington, N.A. The cohesive and adhesive strength of ice. *J. Mater. Sci.* **1983**, *18*, 1455–1465. [CrossRef]

49. Pervier, M.L.A.; Hammond, D. Measurement of the fracture energy in mode I of atmospheric ice accreted on different materials using a blister test. *Eng. Fract. Mech.* **2014**, *1*, 223–232. [CrossRef]
50. Rønneberg, S.; Zhuo, Y.; Laforte, C.; He, J.; Zhang, Z. Interlaboratory Study of Ice Adhesion Using Different Tech-niques. *Coatings* **2019**, *9*, 678. [CrossRef]